Self-consistency in $GW\Gamma$ formalism leading to quasiparticle-quasiparticle couplings

Carlos Mejuto-Zaera * and Vojtěch Vlček †

Department of Chemistry and Biochemistry, University of California, Santa Barbara, California 93106-9510, United States



(Received 9 August 2022; revised 12 October 2022; accepted 13 October 2022; published 26 October 2022)

Within many-body perturbation theory, Hedin's formalism offers a systematic way to iteratively compute the self-energy Σ of any dynamically correlated interacting system, provided one can evaluate the interaction vertex Γ exactly. This is, however, impossible, in general, for it involves the functional derivative of Σ with respect to the Green's function. Here, we analyze the structure of this derivative, splitting it into four contributions and outlining the type of quasiparticle interactions that each of them generate. Moreover, we show how, in the implementation of self-consistency, the action of these contributions can be classified into two: A quantitative renormalization of previously included interaction terms and the inclusion of qualitatively distinct interaction terms through successive functional derivatives of Γ itself. Implementing this latter type of self-consistency can extend the validity of perturbative approximations based on Hedin's equations toward the high interaction limit, as we show in the example of the Hubbard dimer. Our analysis also provides a unifying perspective on the perturbation theory landscape, showing how the T-matrix approach is completely contained in Hedin's formalism.

DOI: 10.1103/PhysRevB.106.165129

Many-body perturbation theory (MBPT) has become widely applied to obtain the description of quasiparticle (QP) energies, in particular, the electron and hole states, and their couplings with fields [1], with a promising perspective for nonequilibrium phenomena [2]. Fundamentally, the perturbation theory framework relates the fully interacting many-body system to a suitably chosen auxiliary (often fictitious) reference one. The latter is selected so the property of interest (e.g., the spectral function $A(\omega)$ representing the QP energies and satellite features) is easy to evaluate and close to that of the physical interacting system. The closeness is typically defined as a perturbation series in terms of a parameter which is small enough to guarantee the convergence and physical accuracy. A successful treatment hinges on the ability to generate the complete perturbative series and practically evaluate it [3,4].

The MBPT framework is formulated around the one-body Green's function G, which is directly related to physical observables, e.g., $A(\omega) \propto \mathrm{Im} G(\omega)$ [5–12]. The reference G_0 is usually computed from a system subject to mean-field interactions. The correction to G_0 , which within MBPT is accessed perturbatively, is then defined via the Dyson equation $\Sigma = G_0^{-1} - G^{-1}$, with the self-energy (SE), Σ , being the central quantity leading to dynamical renormalization. Conceptually, Σ corresponds to an effective scattering potential for the reference QPs, which itself functionally depends on G [1,4]. Further, it recovers the full many-body G in the infinite resummation limit of the Dyson expansion. In practice, multiple approximations to the form of Σ have been explored and applied in various contexts within the MBPT framework [13–24]. Typically, these complementary Ansätze are based

on a choice of the leading scattering mechanism combined with a particular closure of the perturbative expansion. These various methods are often considered to originate from distinct philosophies for generating Σ from the two-particle interactions, how the expansion closure is implemented, and whether self-consistency is necessary.

Among these methods, we revisit here approximations based on Hedin's formalism [25,26], which have been traditionally tied to the context of weak interactions dominated by classical electrodynamic screening and cases when explicit two-particle interactions are merely second (and higher) order effects. We challenge this notion and show how to formulate Hedin's based perturbative approximations applicable toward the high-interaction regime by leveraging a *functional* self-consistency. This has been recognized but explored in only a very limited way so far [27–31], and here we show exactly how it stands apart from the numerical self-consistent solutions for a fixed form of Σ .

Hedin's equations provide a systematic approach to building Σ for a chosen G_0 [4,25,26], relating G to G_0 and the bare Coulomb potential v through the self-energy (SE) Σ and the so-called interaction vertex Γ . The latter term dresses the screened Coulomb potential W with the necessary many-body interactions to form Σ following

$$\Sigma(1,2) = iG(1,\bar{3})W(1,\bar{4})\Gamma(\bar{4},\bar{3},2). \tag{1}$$

We adopt a short-hand notation where space-time coordinate $1 \equiv (\mathbf{r}_1, t_1)$; all coordinates integrated over are indicated by bar. Hedin's equations are closed by interrelating all quantities, and this set of coupled equations should be solved self-consistently. In this paper, we focus on the role of vertex function in this self-consistency. It is directly given in terms

^{*}carlos_mejutozaera@ucsb.edu, cmejutoz@sissa.it

[†]vlcek@ucsb.edu

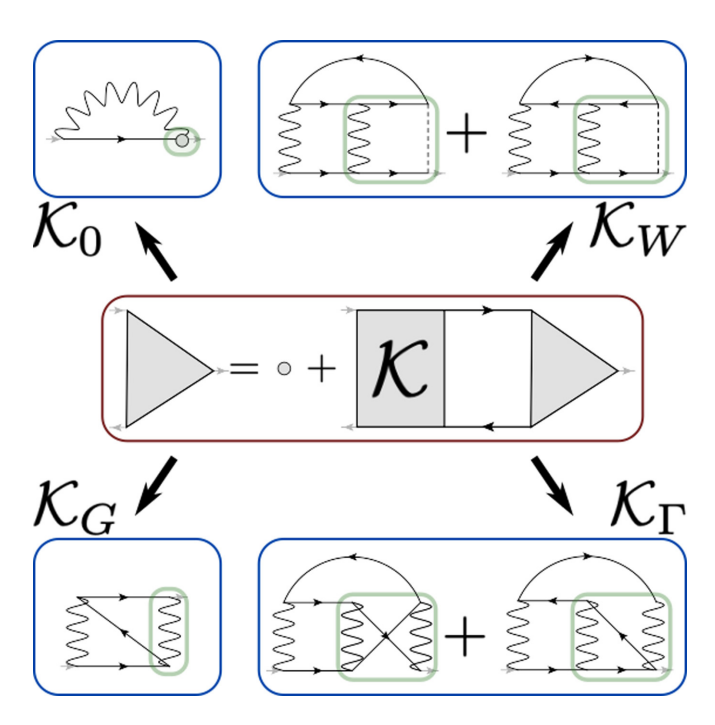


FIG. 1. Components of the interaction kernel \mathcal{K} in the interaction vertex Γ (red box), with diagrams representing the leading order contributions to the self-energy (blue boxes).

of Σ as a resummation:

$$\Gamma(1,2,3) = \delta(1,2)\delta(1,3) + \frac{\delta\Sigma(1,2)}{\delta G(\bar{4},\bar{5})}G(\bar{4},\bar{6})G(\bar{7},\bar{5})\Gamma(\bar{6},\bar{7},3).$$
(2)

We denote the functional derivative on the RHS as the interaction kernel $\mathcal{K}(1, 2, 3, 4) = \delta \Sigma(1, 2) / \delta G(3, 4)$.

The full self-consistent solution requires that the SE in the nth iteration $\Sigma^{(n)}$ enters Eq. (2) and generates a new form of the vertex $\Gamma^{(n+1)}$ via $\mathcal{K}^{(n)}[\Sigma^{(n)}]$. At each additional step, this produces a SE containing new diagrams, making any exact evaluation difficult. We emphasize that this is distinct from a typical self-consistent treatment, in which the functional form of \mathcal{K} is not updated and only numerical convergence is sought. The functional self-consistency between \mathcal{K} and Σ accounts for a resummation in types of many-body interactions.

Practical implementations resort to imposing closure to Hedin's formalism. We identify two typical approaches, which we will explore here: (i) Truncation of the Σ expansion at finite order in interactions or (ii) restricting the appearing diagram topologies that are summed over to all orders. Further, the numerical self-consistency is also typically avoided to lower the computational cost.

First, we illustrate contributions of the kernel $\mathcal{K} = \delta(GW\Gamma)/\delta G$ to both Γ and Σ and impose the truncation: We select the lowest order terms in bare and screened Coulomb interactions (v and W) and take only the first nontrivial step in the resummation of Eq. (2). The corresponding Feynman diagrams for the SE are in Fig. 1, in which the corresponding \mathcal{K} parts are indicated by green rectangles. We distinguish four types of kernels based on how they are generated and interpret them in terms of scattering processes.

(1) $\mathcal{K}_0 = 0$: This is the trivial term in Eq. (2) corresponding to $\Gamma(1,2,3) = \delta(1,2)\delta(1,3)$ and leading to the zeroth order approximation for the SE:

$$\Sigma^{(0)}(1,2) = iG(1,2)W(1,2). \tag{3}$$

It accounts exclusively for a classical, one-body screened Coulomb interaction [32] containing a resummation over polarization diagrams, i.e., the screened exchange diagram in Fig. 1. While greatly improving main QP mean-field features over mean-field (e.g., DFT) results [33–35], it suffers form self-polarization error in W [36–38].

(2) $\mathcal{K}_G = i(\frac{\delta G}{\delta G})W\Gamma$, arising from the variation of G. To generate a nontrivial vertex, it is sufficient to use the zeroth order approximation to Γ . Hence

$$\mathcal{K}_{G}^{(0)}(1,2,3,4) = iW(1,2)\delta(1,3)\delta(2,4). \tag{4}$$

This introduces ladder interactions in $\Gamma^{(1)}$ which enter the recurrence in Eq. (2),

$$\Gamma_G^{(1)}(1,2,3) = iG(1,3)W(1,2)G(2,3),$$
 (5)

where we induce a subscript to indicate from which kernel the vertex is derived. To the lowest order in interaction lines (W), the vertex-corrected SE becomes

$$\Sigma^{(1)}(1,2) = iG(1,\bar{3})W(1,\bar{4})[\delta(\bar{3},2)\delta(\bar{4},2) + iG(\bar{3},\bar{4})W(\bar{3},2)G(\bar{4},2)]. \tag{6}$$

The higher order expansions are illustrated in the Supplemental Material (SM) [39]. Equation (6) corresponds to the two leftmost SE diagrams in Fig. 2 based on \mathcal{K}_0 and \mathcal{K}_G with screened Coulomb interactions. In practice, \mathcal{K}_G introduces additional exchange coupling between the virtual particle-hole (ph) pairs and accounts for excitonic effects, and hence introduces the first nontrivial QP-QP coupling into the approximation. This can be also understood in terms of the charge-charge susceptibility. Within the GW approximation, this contains only local density-density fluctuations, i.e., diagonal terms in the density matrix. These are complemented within the second contribution in Eq. (6) with off-diagonal density matrix contributions to the susceptibility, which are typically referred to as density-matrix fluctuations [30]. Further, it partly corrects the self-polarization error [28,30,40,41].

(3) $\mathcal{K}_W = iG(\frac{\delta W}{\delta G})\Gamma$, arising from the variation of the screened Coulomb potential. Here again, we generate the lowest nontrivial vertex already from $\Sigma^{(0)}$. To the lowest order, W is given by the random phase approximation: $W(1,2) = v(1,2) - iv(1,\bar{3})G(\bar{3},\bar{4})G(\bar{4},\bar{3})W(\bar{4},2)$ and in the first step of Eq. (2) resummation, it yields

$$\Gamma_W^{(1)}(1,2,3) = v(1,\bar{4})G(1,2)W(2,\bar{5})$$

$$\times [G(\bar{4},\bar{5})G(3,\bar{4})G(\bar{5},3)$$

$$+ G(\bar{5},\bar{4})G(3,\bar{5})G(\bar{4},3)]. \tag{7}$$

The vertex represents the second-order correction in terms of interactions (v and W). Note that $\Gamma_W^{(1)}(1,2,3)$ contains explicit particle-particle (pp) and particle-hole (ph) interactions at equal footing [27].

As a result, the lowest order SE in Fig. 1 contains twobody terms, which cannot be reduced to a single propagator interacting with itself through a screened potential W. The leading order terms in Σ from Γ_W are identical to the direct terms found in the *screened* T-matrix expansion [16,42,43]. The higher order screened T matrix is outside of the imposed truncation and results from the second type of closure (resummation restricted to a selected type of diagrams) discussed below. Further, note that it is common to take $\delta W/\delta G \to 0$ as the change of screening is expected to be small, typically in large-scale systems or systems with low screening where $W \sim v$. One is thus tempted to take the limit of $W \to v$ prior to evaluating the vertex. However, to keep the explicit two-body couplings in the SE expression, such a limit has to be taken only *after* Γ has been derived in each step.

(4) $\mathcal{K}_{\Gamma} = iGW(\frac{\delta\Gamma}{\delta G})$ comes from the variation of the vertex in the kernel, which has been, to the best of our knowledge, neglected so far. A nonvanishing \mathcal{K}_{Γ} requires a nontrivial vertex as an input. Clearly, this step can generate an infinite number of diagrams given that Γ is subject to the resummation in Eq. (2). By including only the leading term, we get

$$\begin{split} \frac{\delta}{\delta G(4,5)} \Gamma(1,2,3) &= \frac{\delta}{\delta G(4,5)} [\mathcal{K}(1,2,\bar{6},\bar{7})G(\bar{6},3)G(3,\bar{7})] \\ &= \frac{\delta \mathcal{K}(1,2,\bar{6},\bar{7})}{\delta G(4,5)} G(\bar{6},3)G(3,\bar{7}) \\ &+ \mathcal{K}(1,2,4,\bar{7})G(3,\bar{7})\delta(3,5) \\ &+ \mathcal{K}(1,2,\bar{6},5)G(\bar{6},3)\delta(3,4). \end{split} \tag{8}$$

Since we are interested only in the lowest order expression in interactions (i.e., with the lowest number of v or W terms), we take $\mathcal{K} \approx \mathcal{K}_G^{(0)} = iW$ and further $\delta \mathcal{K}_G^{(0)}/\delta G \approx 0$. As a result,

$$\Gamma_{\Gamma}^{(2)}(1,2,3) = -W(1,\bar{4})G(1,\bar{5})W(2,\bar{5})$$

$$\times [G(\bar{5},3)G(3,\bar{4})G(\bar{4},2)$$

$$+ G(\bar{5},\bar{4})G(\bar{4},3)G(3,2)]. \tag{9}$$

In practice, this expression is analogous to Eq. (7) upon exchange of space-time coordinates. A significant difference is the absence of v terms, i.e., the vertex contains only screened interactions. In the SM, we show how this difference is resolved if one resums the formal Dyson-like equation that defines $\frac{\delta W}{\delta G}$. Note that $\Gamma_{\Gamma}^{(2)}$ represents the same order of perturbation expansion, as $\Gamma_{W}^{(1)}$; it is important that the superscript does not denote the order of the expansion, but enumerates the iteration in the self-consistent cycle. Clearly, the number iterative steps taken in Eq. (2) is not equivalent to the order of the perturbation expansion.

Finally, the resulting SE is in Fig. 1 and corresponds to the exchange form of the T matrix [44]. Here, $\Gamma_{\Gamma}^{(2)}$ corrects the two-body pp and ph interactions in Γ_W by accounting for the Fermionic nature of the QPs.

In the above steps, we derived the leading order terms where we selectively limited the expansion of Γ up to the second order in v and W. This constitutes a particular form of a closure, i.e., finite order truncation. Using this closure, we generated a SE expression containing (lowest order) direct and exchange T-matrix terms for both pp and ph channels. In contrast, such diagrams were previously generated by imposing an Ansatz for the two-body interactions and typically only one of the channels, pp or ph, was applied [16,42,43]. Our

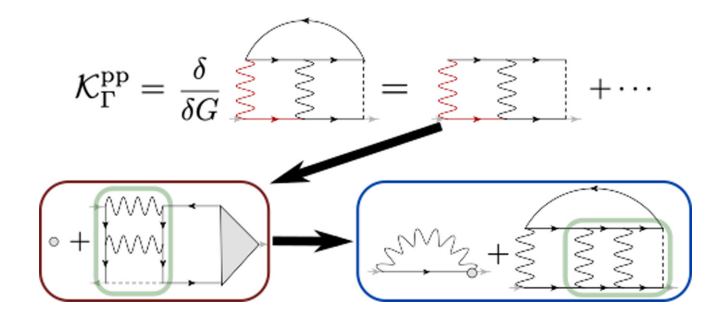


FIG. 2. Graphical sketch for the generation of topologically new diagrams through the functional self-consistency involving the Γ component of the interaction kernel \mathcal{K} . On the first line, Γ portion of the lowest order pp T-matrix-equivalent SE is in black, while the GW component is shown in red. In particular, generation of the second order direct pp T-matrix diagram from the first-order term. The red box encloses the interaction vertex Γ , the blue box the resulting self-energy Σ representing the next lowest order T-matrix SE.

derivation shows that both need to be added simultaneously and at equal footing. All these diagrams are shown in Fig. 1.

Continuing the derivation toward full self-consistency (updating the kernel), K in Eq. (2) will generate a large number of additional diagrams. There is a marked difference in how each nontrivial vertex does this, hinging on whether and how the functional derivative of Γ (the defining component of \mathcal{K}_{Γ}) enters their expression. Indeed, $K_G = W\Gamma$ at each iteration. In turn, \mathcal{K}_W is composed of three terms, two of which do not contain $\delta\Gamma/\delta G$. Hence, \mathcal{K}_G and two out of the three terms in \mathcal{K}_W contribute with diagrams of a particularly restricted structure, essentially further renormalizing the same interaction channels in each iteration (cf. with the starfish algorithm in Ref. [45]). In strong contrast, the terms involving $\delta\Gamma/\delta G$, i.e., one of the terms in \mathcal{K}_W as well as the entire \mathcal{K}_{Γ} , can introduce more complex diagram topologies in each iteration. As we illustrate below, these functional derivatives are critical for expanding the series of explicit QP-QP interactions.

For instance, evaluating the \mathcal{K}_{Γ} kernel as $GW(\delta\Gamma_W^{(1)}/\delta G)$ leads to the next order T-matrix, shown in Fig. 2, along with three additional diagrams that are not shown. Clearly, if the full (functional) self-consistency is sought, the vertex acts as a generator of new diagram topologies and $\delta\Gamma/\delta G$ is constantly expanding with each additional step in the series. Conceptually, this self-consistency potentially extends the convergence radius of the PT expansion, by introducing additional types of diagrams with each iteration. The way the new diagrams arise through \mathcal{K}_W and \mathcal{K}_{Γ} is subtly different, however, \mathcal{K}_W essentially modifying the effective potential through which a given QP interacts with the background particles and holes, while \mathcal{K}_{Γ} can also affect the propagation itself of said QP. This is likely the reason behind previous numerical observations regarding the absence of improvement over GW in approximations including vertex corrections exclusively in the polarization function [46].

It is at this point that the second type of closure becomes apparent: the expansion is formally continued ad infinitum but restricted to a subset of diagrams at each iteration. For example, if we restrict the SE entering $\mathcal K$ to contain only Γ_W -type vertex terms, it consistently generates a series of diagrams

among which we can always identify one that produces the next leading order pp and ph T matrix, as illustrated in Fig. 2 for the case of the pp T-matrix. This analysis demonstrates the critical role of $\frac{\delta \Gamma}{\delta G}$ terms, particularly within \mathcal{K}_{Γ} , as one cannot generate such a series if they are neglected.

Note that this repeated update of the functional form of Γ is distinct from the resummation of Eq. (2) which does not generate the T-matrix type of SE. For instance, in the context of the lowest order T-matrix ladder diagram (upper right corner in Fig. 1), Eq. (2) yields a cascade of *single* pp or ph scatterings. In contrast, the above-described functional self-consistency generates, order by order, a series of repeated pp and ph scattering events that represent the (screened) T-matrix (cf. Fig. 2).

The previous derivation reaches two goals. First, we have shown what types of interactions the leading order terms of $\mathcal K$ introduce in Hedin's construction of the SE. Moreover, we show that this formalism naturally generates SE containing T-matrix types of diagrams, without needing to invoke the Bethe-Salpeter equation, albeit not within a Dyson-type resummation. This exemplifies the role of the recurrence in Eq. (2) and hence provides a unified framework from which to systematically derive and analyze previously developed vertex corrected MBPT approximations [42,43], which have targeted particular phenomenologies. For instance, our derivation indicates that *both* pp and ph T-matrix terms have to be added together into a comprehensive Σ when attempting to apply MBPT systematically. As shown above, practical implementation relies on an appropriate closure.

Naturally, a question arises about what approach is better in practice and how individual vertex terms change the prediction of QP energies. Further, the fact that vertex terms introduce QP-QP interactions suggests that the perturbative treatment may better capture systems with stronger interactions, but the practical limit of the perturbation expansion is unclear. Finally, regardless of the selected closure, one should perform a fully self-consistent calculation which should, in principle, become independent of the starting point.

In the following, we address these questions with self-consistent calculations of a minimal model, the Hubbard dimer at half filling, which became de facto standard test case for MBPT [37,42,47]. While this numerical test is far from exhaustive, it already shows the main qualitative features and demonstrates the role of various vertex terms and types of closures. Details on the simulation parameters and convergence behavior can be found in the Supplemental Material [39] (see also Refs. [48,49] therein).

We perform MBPT calculations on the Hubbard dimer at half filling for different U/t ratios in the span between 1 and 10, starting from symmetric Hartree-Fock mean-field reference (SMF), as well as allowing for symmetry breaking (SBMF). As discussed in the SM, the changing point between the delocalized and atomic behaviours in the dimer occurs at U/t = 2, hence the $U/t \in [1, 10]$ are sufficiently large to study both the weakly and strongly interacting regimes. We present the main results in Fig. 3, which shows the QP energies rescaled by U as a function of U/t for different perturbative methods and mean-field references [50]. For clarity, main QP energies are shown in the lower panels, satellites in the upper panels. We compare to exact diagonalization (ED)

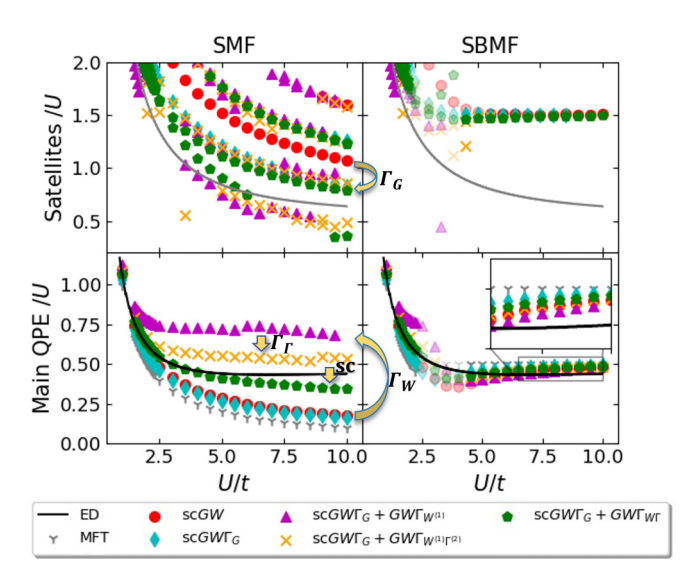


FIG. 3. Quasiparticle energies (QPEs) from the spectral function $A(\omega)$ for the Hubbard dimer at half filling for different U/t values, with main QPEs in the lower panels, satellites in the upper panels. The QPEs are rescaled by U. Shown are ED results as solid lines (main QPE in black, satellite in grey), as well as mean-field and several MBPT approximations as solid markers. Transparent markers in the right panels correspond to calculations where a stable convergence was not possible. Results for a symmetric mean-field (SMF) are shown on the left panels and a symmetry broken mean-field (SBMF) on the right panels. Arrows indicate the effect of the different vertex corrections, and the functional self-consistency (sc), see text for details.

results shown as solid lines (black for the main QP, grey for the satellite), which for the main QP energy show a linear increase as a function of U. The details of the mean-fields and perturbative calculations can be found in the SM.

We employ two reference MF states: SMF and SBMF. Ideally, in a fully self-consistent and resummed MBPT implementation, there should be no dependence on the starting point. However, since we introduce limited types of diagrams and partial self-consistency (see below), this factor cannot be neglected. As we show in detail in the SM, the MF solution for the Hubbard dimer at half filling is unstable to symmetry breaking for U/t > 2, corresponding to the atomic limit. The symmetry broken solution greatly improves the MF total energy, following almost the exact asymptotic behavior for $U/t \to \infty$ and reasonably reproducing the main QP $A(\omega)$ (grey stars in Fig. 3), which in the symmetric MF is independent of U, instead of linear with U. Since the atomic limit is perturbative around t^2/U , the question arises whether SBMF or SMF would be a better reference state for MBPT in the high U/t limit. On the one hand, the energetic closeness of the SBMF to ED is encouraging, but it displays spurious antiferromagnetic order. The exact SE would eliminate it, yet only by including diagrams with spin-flip processes. This limits the usefulness of the SBMF starting point with our current MBPT implementations.

Indeed, as can bee seen comparing both panels in Fig. 3, the main QPE (shown as solid black line for ED) is much more faithfully reproduced in the high U limit by any MBPT

approximation starting from SBMF instead of SMF, while in the intermediate U regime we found trouble converging the different approximations, which we indicate with semitransparent markers in the figure. However, upon closer inspection (see inset in lower right panel), one notices that essentially none of these methods are significantly improving upon the mean-field reference. Satellite features do appear, but their energy is gravely overestimated and their asymptotic distance to the main peak is qualitatively wrong ($\sim U$ instead of constant). The reason behind the lack of improvement is likely the broken symmetry. All the interaction terms and diagrams we include conserve local spin, and thus none of our methods can recover the broken symmetry. This could be potentially remedied within a relativistic framework, in which the total spin projection along z is not a conserved quantity. Our results suggest that the SBMF solution is the optimal symmetry broken description of the model at the high U limit, and we expect a perturbative improvement within the same magnetic phase to be unlikely [51]. Further, we interpret the absence of multiple satellites for the symmetry-broken case (Fig. 3, right upper panel) in our MBPT implementations as another sign that the MF solution is the optimal representation in the SB space. Essentially, none of the perturbative approximations are moving significantly far from the original mean-field solution in the symmetry broken case, resulting in a much simpler, albeit incorrect, satellite structure. Given this limitation, for the rest of the paper we will concentrate exclusively on the results starting from the SMF solution, which as noted above gives the wrong asymptotic behavior of the main QP energy as a function of U.

We first consider the lowest order approximations, performed to self-consistency (sc): scGW (red circles) and $scGW\Gamma_G$ (cyan diamonds). scGW opens the main QP gap from the SMF solution, which is fixed at 2t independently of U. This is the opposite tendency as observed in most ab inito materials [1,26,52] and is a consequence of the Hartree and Fock interactions canceling exactly in the Hubbard model. Furthermore, scGW introduces satellites that systematically overestimate the ED ones (grey solid line) but generally follow a similar behavior with U/t. Upon the introduction of induced density matrix fluctuations and partial removal of the self-polarization error with the sc $GW\Gamma_G$ approximation, we see these satellite features significantly reduce their energy, coming much closer to the ED result. Meanwhile, the main QP energies are barely affected by the introduction of the \mathcal{K}_G kernel. As we will show next, this trend is repeated at all levels of perturbation theory: the K_G kernel, and only this kernel, affects the satellites, leaving the main QP features intact. While for systems with more general interaction terms one would expect some effect on the main QP energies, these findings explain the numerical observations made previously [28,30,40,41].

Next, we include the K_W kernel to leading order [cf. Eq. (7)], which we apply in the $W \to v$ limit as a one-shot correction to the $\operatorname{sc} GW\Gamma_G$ SE, shown as magenta triangles in Fig. 3. We observe that the satellites remain mostly unchanged from $\operatorname{sc} GW\Gamma_G$, up to the appearance of additional spurious satellites at high energy. In strong contrast, the main QP energies experience a huge shift to higher energies, particularly in the large U/t limit. This is not surprising, since

it is in this regime where the pp and ph interaction diagrams from \mathcal{K}_W become dominant. While the main QP energies are clearly overestimated, there is an encouraging change in the asymptotic behavior with U/t, resembling much stronger the correct flat $(\sim U)$ one.

The systematic overestimation of the QP energies gets significantly corrected by recovering the exchange diagrams in \mathcal{K}_{Γ} . We evaluate these also to leading order [cf. Eq. (9)] in the $W \rightarrow v$ limit and add them as one-shot correction to the SE (yellow crosses in Fig. 3). This implementation keeps the promising asymptotic behavior (and satellite peaks), while pushing the main QP energies much closer to the ED results. It is in this sense that we extend the qualitative validity of MBPT approximations toward the high interaction limit by including diagrams through \mathcal{K}_{Γ} . Further, this indicates that we are adding the most important missing interactions in the SMF model, namely, the explicit twobody (exchange corrected) Coulomb interactions, in both pp and ph channels. This compares favorably with previous studies within the T-matrix approach, which could not observe this improvement in the large U/t limit since they added either the pp or the ph channel, but not both together [42].

Finally, we want to illustrate the effect of the self-consistency in \mathcal{K}_{Γ} , namely, the introduction of a full resummation of a subset of diagrams which arise naturally through $\frac{\delta \Gamma}{\delta G}$ in successive iterations of Hedin's equations. Here, we resum all T-matrix type diagrams, which we add as one-shot correction to the $\mathrm{sc}GW\Gamma_G$ SE (green pentagons in Fig. 3), accounting thus for the leading order terms in all kernels \mathcal{K} , as well as both types of self-consistencies (numerical and functional). The satellite features improve slightly toward the ED limit, but the most important change is undoubtedly the effect on the main QP energies. These become essentially exact up to U/t=4, showing an extension of the qualitative and quantitative validity of MBPT approximations toward the high interaction limit, going through the formally strongly correlated point at U/t=2.

Still, the persistent satellite overestimation and appearance of spurious satellites suggest that renormalization of the new scattering channels to the correct quantitative energy scale is still missing. Moreover, as can be seen at the main QP energies for U/t > 5, further diagrams are likely needed to recover the exact results. This may require resummation within the diagram classes already introduced, such as by including the T-matrix-like Σ into the self-consistency procedure, including the \mathcal{K}_W and \mathcal{K}_Γ contributions to W, or introducing higher order functional derivative terms in \mathcal{K} . We attempted including both the leading order and resummed versions of $\Sigma[\Gamma_W, \Gamma_\Gamma]$ into the self-consistency procedure (see SM), but the resulting MBPT method does not converge to a stable Green's function for U/t > 5, in contrast to the U/t < 5 regime.

Nonetheless, the numerical results support our theoretical conclusions: The higher order functional derivative terms in \mathcal{K}_Γ introduce additional classes of diagrams which are necessary to extend the qualitative applicability of MBPT toward the high interaction limit. In other words, \mathcal{K}_Γ affects the convergence radius of the perturbative expansion. Meanwhile, resummations within a diagram class, be it within the solution of a Dyson-like equation or in the self-consistency

of \mathcal{K}_0 , \mathcal{K}_G , and \mathcal{K}_W , fixes the quantitative agreement and hence is important for the reliability of the converged solution.

For completeness, we conclude with a note of caution: As as our results above convincingly suggest, adding the $\mathcal{K}_{W,\Gamma}$ terms can extend the validity of Hedin-based MBPT approximations from the weakly to the highly interacting limit. Still, if the system studied presents strong electronic correlation between these two limits, e.g., at a phase transition, then a perturbative implementation of Hedin's expansion is not justified. Higher order perturbative corrections can only constrain the phase space region around strongly correlated points where MBPT is unreliable. Nevertheless, as we have shown in the Hubbard dimer, this can account for a significant portion of dynamical correlation in a numerically stable fashion.

It is worth noting that Hedin's equations per se are not perturbative, and indeed the exact SE of any system satisfies them. Hence, one can capture QP couplings within the interaction vertex also in strongly correlated systems, provided a nonperturbative SE approximation is employed. This can be done, for instance, within the parquet formalism, whose explicit equivalence with Hedin's equations has been recently shown in Ref. [53]. Practical implementations of this framework involve approximations of the fully irreducible four-point vertex Λ , instead of approximating the functional derivative $\frac{\delta \Sigma}{\delta G}$. Choosing a nonperturbative approximation for Λ, e.g., leveraging the infinite dimensional limit as in the dynamical vertex approximation [54], thus allows accessing strong correlation. These approximations to Λ have typically steep computational scalings, and hence methods based on approximating $\frac{\delta \Sigma}{\delta G}$, such as the perturbative expansions in this paper, are an attractive alternative to study materials ab initio. Some of the perturbative expansions previously considered in the literature have been formulated in terms of physically motivated heuristics, such as interpolating between high and low density limits [42]. Our paper instead suggests using the functional self-consistency provided by the functional derivatives of the interaction vertex itself as a guiding principle to choose diagrammatic closures that can result in systematically improvable approximations, as shown here for the Hubbard dimer.

In this paper, we analyzed the structure of the interaction vertex Γ in regard to its role as generator of QP interactions, and thus bridge between the mean-field and fully interacting Green's functions in Hedin's formalism for manybody perturbation theory. We identified the diagram types generated by each component of the interaction kernel K = $\frac{\delta \Sigma}{\delta G}$, highlighting the effect of each one on the different features the experimentally accessible spectral function. Further, we outlined the two distinct types of self-consistency encountered in the formalism: That carried by the first elements of the kernel $\mathcal{K}_{0,G,W}$, which accounts for interaction renormalization and quantitative improvement of the description, and that governed by $\mathcal{K}_{\Gamma} \propto \frac{\delta \Gamma}{\delta G}$, which is responsible for generating new diagrams in each iteration, thus potentially extending the validity of the perturbative approach through the phase diagram. Finally, this analysis allowed us to present a unified perspective on perturbative Ansätze, in particular, showing how the T-matrix approach is generated within Hedin's formalism, and realizing the importance of including both particle-particle and particle-hole channels in the calculation. We hope this view on MBPT will help the development of scalable implementations toward the highly interacting limit, and look forward to the promising stochastic implementation of the $\mathcal{K}_{W,\Gamma}$ terms to large realistic systems [30] in which to test the transferability of our findings for the Hubbard dimer.

Insightful discussions and comments from A. Förster, G. Kotliar, E. K. U. Gross, J. Skolimowski, and M. Fabrizio are gratefully acknowledged. The theoretical analysis of vertex corrections was supported by the NSF CAREER award (DMR-1945098). The implementation, the detailed numerical analysis, and the preparation of the publicly available code is based upon work supported by the U.S. Department of Energy, Office of Science, Office of Advanced Scientific Computing Research, Scientific Discovery through Advanced Computing (SciDAC) program under Award No. DE-SC0022198. This research used resources of the National Energy Research Scientific Computing Center, a DOE Office of Science User Facility supported by the Office of Science of the U.S. Department of Energy under Contract No. DE-AC02-05CH11231 using NERSC Award No. BES-ERCAP0020089.

G. Onida, L. Reining, and A. Rubio, Electronic excitations: Density-functional versus many-body Green's-function approaches, Rev. Mod. Phys. 74, 601 (2002).

^[2] E. Perfetto, Y. Pavlyukh, and G. Stefanucci, Real-Time GW: Toward an *Ab Initio* Description of The Ultrafast Carrier and Exciton Dynamics in Two-Dimensional Materials, Phys. Rev. Lett. 128, 016801 (2022).

^[3] A. A. Abrikosov, L. P. Gorkov, and I. E. Dzyaloshinski, *Methods of Quantum Field Theory in Statistical Physics* (Dover Publications, New York, 1975), Vol. 85.

^[4] R. M. Martin, L. Reining, and D. M. Ceperley, *Interacting Electrons: Theory and Computational Approaches* (Cambridge University Press, Cambridge, 2016).

^[5] S. Hüfner, J. Osterwalder, T. Riesterer, and F. Hulliger, Photoemission and inverse photoemission spectroscopy of NiO, Solid State Commun. 52, 793 (1984).

^[6] M. Sander, L. A. Chewter, K. Müller-Dethlefs, and E. W. Schlag, High-resolution zero-kinetic-energy photoelectron spectroscopy of nitric oxide, Phys. Rev. A 36, 4543 (1987).

^[7] L. Chewter, M. Sander, K. Müller-Dethlefs, and E. Schlag, High resolution zero kinetic energy photoelectron spectroscopy of benzene and determination of the ionization potential, J. Chem. Phys. 86, 4737 (1987).

^[8] P. Puschnig, S. Berkebile, A. J. Fleming, G. Koller, K. Emtsev, T. Seyller, J. D. Riley, C. Ambrosch-Draxl, F. P. Netzer, and

- M. G. Ramsey, Reconstruction of molecular orbital densities from photoemission data, Science 326, 702 (2009).
- [9] C. Vozzi, M. Negro, F. Calegari, G. Sansone, M. Nisoli, S. De Silvestri, and S. Stagira, Generalized molecular orbital tomography, Nat. Phys. 7, 822 (2011).
- [10] G. Wu, P. Hockett, and A. Stolow, Time-resolved photoelectron spectroscopy: From wavepackets to observables, Phys. Chem. Chem. Phys. 13, 18447 (2011).
- [11] D. Lüftner, T. Ules, E. M. Reinisch, G. Koller, S. Soubatch, F. S. Tautz, M. G. Ramsey, and P. Puschnig, Imaging the wave functions of adsorbed molecules, Proc. Natl. Acad. Sci. USA 111, 605 (2014).
- [12] J. S. Zhou, L. Reining, A. Nicolaou, A. Bendounan, K. Ruotsalainen, M. Vanzini, J. J. Kas, J. J. Rehr, M. Muntwiler, V. N. Strocov, F. Sirotti, and M. Gatti, Unraveling intrinsic correlation effects with angle-resolved photoemission spectroscopy, Proc. Natl. Acad. Sci. USA 117, 28596 (2020).
- [13] R. Del Sole, L. Reining, and R. W. Godby, $GW\Gamma$ approximation for electron self-energies in semiconductors and insulators, Phys. Rev. B **49**, 8024 (1994).
- [14] M. Shishkin, M. Marsman, and G. Kresse, Accurate quasiparticle spectra from self-consistent GW calculations with vertex corrections, Phys. Rev. Lett. 99, 246403 (2007).
- [15] M. Hellgren, N. Colonna, and S. de Gironcoli, Beyond the random phase approximation with a local exchange vertex, Phys. Rev. B 98, 045117 (2018).
- [16] M. Springer, F. Aryasetiawan, and K. Karlsson, First-Principles T-Matrix Theory with Application to the 6 eV Satellite in Ni, Phys. Rev. Lett. 80, 2389 (1998).
- [17] F. Bruneval and M. A. Marques, Benchmarking the starting points of the GW approximation for molecules, J. Chem. Theory Comput. 9, 324 (2013).
- [18] X. Blase, C. Attaccalite, and V. Olevano, First-principles GW calculations for fullerenes, porphyrins, phtalocyanine, and other molecules of interest for organic photovoltaic applications, Phys. Rev. B 83, 115103 (2011).
- [19] V. Vlček, D. Neuhauser, E. Rabani, and R. Baer, Stochastic *GW* calculations for molecules, J. Chem. Theory Comput. **13**, 4997 (2017).
- [20] D. Zhang, N. Q. Su, and W. Yang, Accurate quasiparticle spectra from the T-matrix self-energy and the particle–particle random phase approximation, J. Phys. Chem. Lett. 8, 3223 (2017).
- [21] F. D. Vila, J. J. Rehr, J. J. Kas, K. Kowalski, and B. Peng, Real-time coupled-cluster approach for the cumulant Green's function, J. Chem. Theory Comput. 16, 6983 (2020).
- [22] M. Tzavala, J. J. Kas, L. Reining, and J. J. Rehr, Nonlinear response in the cumulant expansion for core-level photoemission, Phys. Rev. Res. 2, 033147 (2020).
- [23] V. Vlček, E. Rabani, and D. Neuhauser, Quasiparticle spectra from molecules to bulk, Phys. Rev. Mater. 2, 030801(R) (2018).
- [24] J. Lischner, G. K. Pálsson, D. Vigil-Fowler, S. Nemsak, J. Avila, M. C. Asensio, C. S. Fadley, and S. G. Louie, Satellite band structure in silicon caused by electron-plasmon coupling, Phys. Rev. B 91, 205113 (2015).
- [25] L. Hedin, New method for calculating the one-particle Green's function with application to the electron-gas problem, Phys. Rev. 139, A796 (1965).
- [26] F. Aryasetiawan and O. Gunnarsson, The *GW* method., Rep. Prog. Phys. **61**, 237 (1998).

- [27] A. Schindlmayr and R. W. Godby, Systematic Vertex Corrections Through Iterative Solution of Hedin's Equations Beyond the GW Approximation, Phys. Rev. Lett. **80**, 1702 (1998).
- [28] A. Grüneis, G. Kresse, Y. Hinuma, and F. Oba, Ionization Potentials of Solids: The Importance of Vertex Corrections, Phys. Rev. Lett. **112**, 096401 (2014).
- [29] A. L. Kutepov, Self-consistent solution of Hedin's equations: Semiconductors and insulators, Phys. Rev. B 95, 195120 (2017).
- [30] V. Vlček, Stochastic vertex corrections: Linear scaling methods for accurate quasiparticle energies, J. Chem. Theory Comput. 15, 6254 (2019).
- [31] Y. Wang, P. Rinke, and X. Ren, Assessing the $G_0W_0\Gamma_0^{(1)}$ Approach: Beyond G_0W_0 with Hedin's full second-order self-energy contribution, J. Chem. Theory Comput. 17, 5140 (2021).
- [32] Containing a resummation over polarization diagrams.
- [33] M. S. Hybertsen and S. G. Louie, First-Principles Theory of Quasiparticles: Calculation of Band Gaps in Semiconductors and Insulators, Phys. Rev. Lett. 55, 1418 (1985).
- [34] M. S. Hybertsen and S. G. Louie, Electron correlation in semiconductors and insulators: Band gaps and quasiparticle energies, Phys. Rev. B 34, 5390 (1986).
- [35] R. W. Godby, M. Schlüter, and L. J. Sham, Accurate Exchange-Correlation Potential for Silicon and Its Discontinuity on Addition of an Electron, Phys. Rev. Lett. 56, 2415 (1986).
- [36] W. Nelson, P. Bokes, P. Rinke, and R. W. Godby, Self-interaction in Green's-function of the hydrogen atom, Phys. Rev. A 75, 032505 (2007).
- [37] P. Romaniello, S. Guyot, and L. Reining, The self-energy beyond GW: Local and nonlocal vertex corrections, J. Chem. Phys. 131, 154111 (2009).
- [38] F. Aryasetiawan, R. Sakuma, and K. Karlsson, *GW* approximation with self-screening correction, Phys. Rev. B **85**, 035106 (2012).
- [39] See Supplemental Material at http://link.aps.org/supplemental/ 10.1103/PhysRevB.106.165129 for a note on the resummation of $\delta W/\delta G$, a derivation of Hedin's equations in orbital space, the concrete expressions for our perturbative approximations, some comments on the Hubbard dimer mean-field, our simulation parameters, and a.zip file with the data in Fig. 3.
- [40] E. Maggio and G. Kresse, GW vertex corrected calculations for molecular systems, J. Chem. Theory Comput. **13**, 4765 (2017).
- [41] C. Mejuto-Zaera, G. Weng, M. Romanova, S. J. Cotton, K. B. Whaley, N. M. Tubman, and V. Vlček, Communication: Are multi-quasiparticle interactions important in molecular ionization? J. Chem. Phys. 154, 121101 (2021).
- [42] P. Romaniello, F. Bechstedt, and L. Reining, Beyong *GW* approximation: Combining correlation channels, Phys. Rev. B **85**, 155131 (2012).
- [43] D. Nabok, S. Blügel, and C. Friedrich, Electron–plasmon and electron–magnon scattering in ferromagnets from first principles by combining *GW* and *GT* self-energies, npj Comput. Mater. 7, 1 (2021).
- [44] This is in complete analogy to how the Fock diagram can be constructed from the Hartree term; hence we refer to this topological analogy as exchange-equivalent diagram.
- [45] F. Tandetzky, J. K. Dewhurst, S. Sharma, and E. K. U. Gross, Multiplicity of solutions to *GW*-type approximations, Phys. Rev. B **92**, 115125 (2015).

- [46] A. M. Lewis and T. C. Berkelbach, Vertex corrections to the polarizability do not improve the *GW* approximation for the ionization potential of molecules, J. Chem. Theory Comput. **15**, 2925 (2019).
- [47] S. Di Sabatino, P.-F. Loos, and P. Romaniello, Scrutinizing GW-based methods using the Hubbard dimer, Front. Chem. 9 (2021).
- [48] P. Pulay, Convergence acceleration of iterative sequences. the case of scf iteration, Chem. Phys. Lett. **73**, 393 (1980).
- [49] P. Pulay, Improved scf convergence acceleration, J. Comput. Chem. 3, 556 (1982).
- [50] We identify the main QP peak as the one continuously evolving from the only spectral feature in

- the U/t = 0 limit upon increase of the Coulomb interaction.
- [51] Alternatively, one could include a symmetry breaking term h into the MBPT expansion, and take $h \to 0$ at the end of the calculation. Such a driven solution could overcome this issue, in principle, but it requires careful treatment.
- [52] D. Golze, M. Dvorak, and P. Rinke, The GW compendium: A practical guide to theoretical photoemission spectroscopy, Front. Chem. 7, 377 (2019).
- [53] F. Krien, A. Kauch, and K. Held, Tiling with triangles: Parquet and $GW\gamma$ methods unified, Phys. Rev. Res. 3, 013149 (2021).
- [54] A. Toschi, A. A. Katanin, and K. Held, Dynamical vertex approximation: A step beyond dynamical mean-field theory, Phys. Rev. B 75, 045118 (2007).